Journal of Naval Architecture and Marine Engineering
June, 2005
http://jname.8m.net

APPLICATION OF LOW-Re TURBULENCE MODELS FOR FLOW SIMULATIONS PAST UNDERWATER VEHICLE HULL FORMS

P. Jagadeesh[1] and K. Murali[2]

[1] Research scholar, Department of Ocean Engineering, Indian Institute of Technology Madras, Chennai, India.
Ph : 0091 44 22574816, Fax : 0091 44 22574816, E mail : jagadeeshiitm@yahoo.com

[2] Assistant professor, Department of Ocean Engineering, Indian Institute of Technology Madras, Chennai, India.
Ph : 0091 44 22574816, Fax : 0091 44 22574816, E mail : murali@iitm.ac.in

Abstract

Minimum power requirement is one of the important design criteria for successful operation of underwater vehicles. CFD based prediction and estimation of power requirement is increasingly carried out in practice. However, reliable prediction depends on suitable turbulence models. This paper presents a comparative assessment of four low Reynolds number (low-Re) k- ε models for computation of hydrodynamic forces on underwater vehicle hull forms. The low-Re models are being considered more suitable for underwater axisymmetric bodies due to the following merits (i) they have no wall function approximations, (ii) they could compute low turbulence levels such as in the viscous sub-layer and (iii) they could account for the effect of damped turbulence. The low-Re models used in the present study are namely the models of Abe-Kondoh-Nagano (k- ε AKN), Chang-Hsieh-Chen (k- ε CHC), Launder-Sharma (k- ε LS), and Yang-Shih (k- ε YS). It has been found that the k- ε AKN low-Re model consistently provided superior performance in predicting the flow characteristics around underwater vehicle hull forms.

Keywords: Axisymmetric bodies, autonomous underwater vehicle, CFD, damping functions, low Reynolds k- ε models, QUICK scheme

NOMENCLATURE

C_{dv} total volumetric drag coefficient D/ $(0.5\rho\nabla^{2/3} U^2_{ref})$
C_{fv} volumetric friction drag coefficient F/ $(0.5\rho\nabla^{2/3} U^2_{ref})$
C_p surface pressure coefficient P_d / $(0.5\ \rho\ U^2_{ref})$
C_{pv} volumetric pressure drag coefficient P/ $(0.5\rho\nabla^{2/3} U^2_{ref})$
D total drag force on body
F friction drag of body
k turbulent kinetic energy
L length of body
P pressure drag of body
P_d pressure on the body surface
R radius of any point above body surface
R_o radius of point on body surface
R_e Reynolds number based on length
R_G grid refinement ratio
R_{max} maximum radius of body
T_u turbulent intensity
u velocity component in axial direction
u_ε Kolmogorov mean velocity $(\gamma\varepsilon^{1/4})$
u_τ resultant friction velocity (τ_ω/ρ)
u_{ref} velocity of the body
v velocity component in radial direction
X axial distance from nose
y normal distance from body surface
y^+ dimensionless distance normal to body surface, $y+ = y u_r/\nu$
ε energy dissipation rate
μ dynamic viscosity of fluid
μ_t turbulent viscosity of fluid
ν kinematic viscosity of fluid
ρ mass density of fluid
τ_w wall shear stress
∇ volume of body
$c_\mu, c_{\varepsilon1}, c_{\varepsilon2}, \sigma_k, \sigma_\varepsilon$ model constants
$f_\mu, f_{\varepsilon1}, f_{\varepsilon2}$ damping functions

1. Introduction

Simulation of flows past underwater vehicle hull forms is of considerable importance in marine hydrodynamics. This is mainly due to lack of reliable and sufficiently accurate experimental data. Generation of quality experimental data requires a large number of hull forms and experimental facilities. In the last two decades, different areas of incompressible flow modeling - including grid

generation techniques, solution algorithms and turbulence modeling, and computer hardware capabilities - have witnessed tremendous development. In view of these developments, Computational fluid dynamics (CFD) can offer a cost-effective solution to many problems in underwater vehicle hull forms. However, effective utilization of CFD for marine hydrodynamics depends on proper selection of turbulence model, grid generation and boundary resolution. On the other hand grid generation and boundary layer resolution depends on the kind of turbulence model that is used in a solution process. However, it can be said that the main issue is turbulence modeling and grid generation and boundary layer resolution are sub-issues. This paper intends to address these issues by way of testing a commercial CFD code that solves the Reynolds-averaged Navier-Stokes (RANS) equation against available data.

Turbulence modeling is still a necessity as even with the emergence of high performance computing analysis of complex flows by direct numerical simulations (DNS) is untenable. The peer approach, the large-Eddy simulation (LES), still remains expensive. Hence, simulation of underwater hydrodynamics continues to be based on the solution of the Reynolds-averaged Navier-Stokes (RANS) equations. A recent trend in RANS equations based turbulence modeling is the introduction of low-Re models by several authors. The low-Re models have no wall functions as they compute the entire boundary layer including the viscous sub-layer. Various researchers used turbulence modeling to simulate flow around axisymmetric bodies since late seventies. Patel and Chen (1986) made an extensive review of the simulation of flow past axisymmeric bodies. Choi and Chen (1990) gave calculation method for the solution of RANS equation, together with k- ε turbulence model. This procedure has been applied for numerical simulation of complete turbulent flow field past axisymmetric bodies (AFTERBODY1, AFERBODY2, AFTERBODY3 and AFTERBODY5). Sarkar et al. (1997) used a low-Re k- ε model of Lam and Bremhorst (1981) for simulation of flow past underwater axisymmetric bodies. This model is known as k- ε L&B in the literature. It has been reported that the k- ε L&B had shown excellent performance in prediction of drag and pressure coefficient compared to standard closure models (k- ε Standard and k- ε RNG).

The review of literature indicates that the low-Re k- ε models are not fully explored as for as application to underwater hydrodynamics is concerned. The investigation and standardization of an efficient turbulence modeling technique for simulation of the flow past underwater bodies would greatly reduce the number of physical model tests and help in drastically cutting the cost and time consumption. The basic criteria for such techniques are the closure approximation through a turbulence model. The low-Re k- ε models such as Abe-Kondoh-Nagano (1994), Chang-Hsieh-Chen (1995) Launder-Sharma (1974) and Yang-Shih (1993) do not appear to have been fully used for simulation of the flow past the entire length of underwater vehicle hull forms. In the literature these models are known as k- ε AKN, k- ε CHC, k- ε LS and k- ε YS respectively. This paper presents investigation of application of the above four two-equation RANS turbulence models to underwater hull forms. The investigation tries to evaluate their ability to model turbulence by way computing and comparing drag, surface pressure distribution, pressure boundary layers and velocity boundary layers. The comparisons are carried out with past data [Huang et al., (1978)]. Flow simulations were carried out at a Reynolds number (Re) of the order 10^6 and correspond to a design speed of 5 m/s for underwater vehicles.

2. Governing Equations

The Low-Re k-ε turbulence modeling used in the Reynolds-averaged Navier-Stokes equation is based on the following k and ε equations,

$$\rho \frac{Dk}{Dt} = \frac{\partial}{\partial x_i}\left[\left(\mu + \frac{\mu_t}{\sigma_k}\right)\frac{dk}{dx_i}\right] + G_k - \rho\varepsilon - D \tag{1}$$

$$\rho \frac{D\varepsilon}{Dt} = \frac{\partial}{\partial x_i}\left[\left(\mu + \frac{\mu_t}{\sigma_\varepsilon}\right)\frac{d\varepsilon}{dx_i}\right] + \frac{c_{\varepsilon 1} f_1 G_k \varepsilon}{k} - \frac{c_{\varepsilon 2} f_1 \varepsilon^2}{k} + E \tag{2}$$

where,

$$G_k = 2\mu_t S^2 = 0.5\mu_t\left(\frac{\partial u_i}{\partial x_j} + \frac{\partial u_j}{\partial x_i}\right)^2 \quad \text{and} \quad \mu_t = C_\mu \rho f_\mu \frac{k^2}{\varepsilon} \tag{3}$$

where μ_t is known as the turbulent viscosity. The reader is advised to refer to nomenclature for definition of the above variables.

The model constants and damping functions for the four low-Re k-ε models considered for this study are given in Table. I and Table. II respectively.

Table I: Model constants in Low-Re Number k-ε models

S. No.	Model	C_μ	$C_{\varepsilon 1}$	$C_{\varepsilon 2}$	σ_k	σ_ε
1.	Abe-Kondoh-Nagano (AKN)	0.09	1.50	1.90	1.40	1.40
2.	Chang-Hsieh-Chen (CHC)	0.09	1.44	1.92	1.00	1.30
3.	Launder-Sharma (LS)	0.09	1.44	1.92	1.00	1.30
4.	Yang-Shih (YS)	0.09	1.44	1.92	1.00	1.30

Table II. Damping fuctions in Low-Re Number k-ε models

Model	f_μ	$f_{\varepsilon 1}$	$f_{\varepsilon 2}$
AKN	$\left[1-\exp\left(\frac{-y^k}{14}\right)\right]^2\left[1+\frac{5}{R_T^{3/4}}\exp\left\{-\left(\frac{R_T}{200}\right)^2\right\}\right]$	1	$\left[1-\exp\left(\frac{-y^k}{3.1}\right)\right]^2\left[1-0.3\exp\left\{-\left(\frac{R_T}{6.5}\right)^2\right\}\right]$
CHC	$\left[1.0-\exp\left(-0.0215\ R_y\right)\right]^2\left(1+\frac{31.66}{R_T^{5/4}}\right)$	1	$\left[1-0.01\exp\left(R_T^2\right)\right]\left[1-\exp\left(-0.0631\ R_y\right)\right]$
LS	$\exp[-3.4/(1+R_T/10)^2$	1	$1-0.3\exp(-R^2{}_T)$
YS	$\left(1+\frac{c_k}{\sqrt{R_T}}\right)*\left[1-\exp\left(\begin{matrix}-1.5x10^{-4}R_y-\\5.0x10^{-7}R_y^3-\\1.0x10^{-10}R_y^5\end{matrix}\right)\right]^{1/2}$	$\frac{1}{1+\frac{c_k}{\sqrt{R_T}}}$	$\frac{1}{1+\frac{c_k}{\sqrt{R_T}}}$

Note: $c_k = 1.0$, $R_T = k^2/(\nu\varepsilon)$, $R_y = yk^{1/2}/\nu$ and $y^k = u_\varepsilon y/\nu$

3. Boundary Conditions

The appropriate boundary conditions for the underwater hydrodynamics problem are,

- At the upstream inlet ($x=x_i$):

$$u = u_i\ ;\quad k = k_i\ ;\quad \varepsilon = \varepsilon_i\ ;\ \text{with}\quad k_i = 1.5\,(T_u)^2 \text{ and } \quad \varepsilon_i = C_\mu\,\frac{k_i^{1.5}}{l}$$

The Turbulent intensity T_u and length scale $l_i = 0.001L$ (L=length of the body), as per Choi and Chen (1990).

- At the downstream boundary: p=0.
- The surface boundary conditions used on the hull from are as specified in the Table III.
- On the upper boundary: $u = u_i$.
- at the centerline (excluding on the axisymmetric body) $v = 0$, $u_{,y} = k_{,y} = \varepsilon_{,y} = 0$

4. Methodology

4.1 Computational method and domain

The axisymmetric problem with appropriate boundary conditions is solved over a finite computational domain. The computational domain extended 0.7L upstream of the leading edge of the axisymmetric body, 0.6L above the body surface and 5.5L downstream from the trailing edge; where L is the overall

length of the body. The solution domain (Figure 1) is found large enough to capture the entire viscous-inviscid interaction and the wake development.

A finite volume method was employed to obtain a solution of the spatially averaged Navier-Stokes equations. The coupling between the pressure and velocity fields was achieved using SIMPLE technique. A QUICK scheme was used for the convection and the central-differencing scheme for diffusion terms. Calculations were carried out on a SGI Irix machine working at 300 MHZ. However, extending the same study to full 3D modeling will require extensive computing resources.

Table III: Additional D and E terms and boundary condtions

Model	D	E	Boundary conditions
AKN	0	0	k = 0 ; $\varepsilon = 2\nu\left(\frac{\partial\sqrt{k}}{\partial y}\right)^2$
CHC	0	0	k = 0 ; $\varepsilon = \nu\left(\frac{\partial^2 k}{\partial y^2}\right)$
LS	$2\nu\left(\frac{\partial\sqrt{k}}{\partial y}\right)^2$	$2\nu_t\nu\left(\frac{\partial^2 u}{\partial y^2}\right)^2$	k = 0; ε = 0
YS	0	$\nu_t\nu\left(\frac{\partial^2 u}{\partial y^2}\right)^2$	k = 0; $\varepsilon = \nu\left(\frac{\partial^2 k}{\partial y^2}\right)$

In all the above low-Re turbulence models, y is the normal distance from the body wall.

4.2 Grid generation

A body-fitted H-type grid was obtained using FLUENT® preprocessor GAMBIT®. In external flow simulations using low-Re turbulence models (k-ε AKN, k-ε CHC, k-ε LS and k-ε YS) the computational grid should be in such a way that sufficient number of grid points lie with in the laminar sublayer of the ensuing boundary layer. In order to ensure this, usually the y^+ criterion is used. y^+ is a non-dimensional distance from the body wall and is defined as $y^+ = yu_\tau/\nu$, where $u_\tau = \tau_\omega/\rho$ is friction velocity and ν kinematic viscosity. The y+ criterion states that that first grid point normal to the body wall should not lie beyond $y^+ = 4.0$ and for reasonable accuracy at least five points should lie with in $y^+ = 11.5$ [Lam and Bremhorst (1981)]. In the present investigation all computational grids are generated with a first grid point at $y^+=2$ and five nodes with in the laminar sublayer ($y^+=11.5$). The outer grid consists 101 nodes placed along the body profile with a growth rate of 1:1 and 48 nodes in the radial direction with a growth rate of 1:1.17 beyond laminar sublayer to ensure grid convergence. The respective grid numbers (NG) and the growth rate (GR) are given in Fig. 1. A typical grid layout around AFTERBODY1 is shown in Fig. 2. The complete details of the domain and grid are given in Table IV.

4.3 Selection of underwater bodies (AUV) for testing

In order to study the comparative performance of the above turbulence models simulations were undertaken for the flow past two underwater vehicle hull forms: AFTERBODY1 and AFTERBODY2. The main reasons for the choice of these bodies were two fold:

These are widely used body profiles for sub-surface marine vehicles ranging from typical torpedo (underwater missile) to most commonly used autonomous underwater vehicles.

For these bodies reliable experimental data are already available for rigorous testing of numerical simulation results [Huang et al., (1978)] at the following Reynolds numbers: AFTERBODY1, Re = 6.8×10^6 and AFTERBODY2, Re = $6.6 \times 10^{6.}$

5. Results and Discussion

5.1 Grid independence analysis

A grid independence analysis was conducted using four meshes with grid refinement ratio $R_G = \sqrt{2}$. For industrial CFD, $R_G = 2$ may often be too large. A good alternative is hence $R_G = \sqrt{2}$, as it provides

fairly large parameter refinement ratio and at least enables prolongation of the coarse-parameter solution as an initial guess for the fine parameter solution (Stern etal., 1999). Computations were carried out for each k-ε AKN turbulence model at a free-stream velocity of 5 m/s. Table V details the type of mesh indicating number of nodes, predicted volumetric drag coefficient and percentage deviation. The table indicates that the solution convergence for Grid 2 and, Grid 2 and Grid 3 have predicted almost identical coefficients.

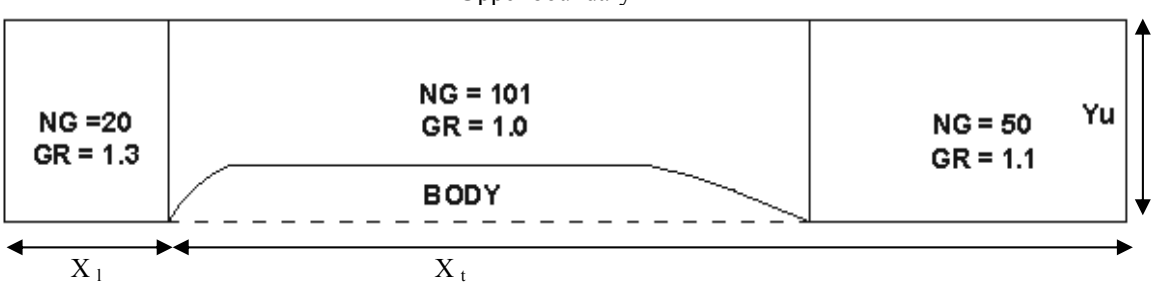

Fig. 1: Grid distribution

Table IV: Grid details

Type of the Axisymmetric body	Grid Low-Re	X_l (leading edge) Meters	X_t (trailing edge) Meters	Y_u (top point) Meters
AFTERBODY1	171 x 48	-2.23	16.80	1.77
AFTERBODY2	171 x 48	-2.23	16.80	1.80

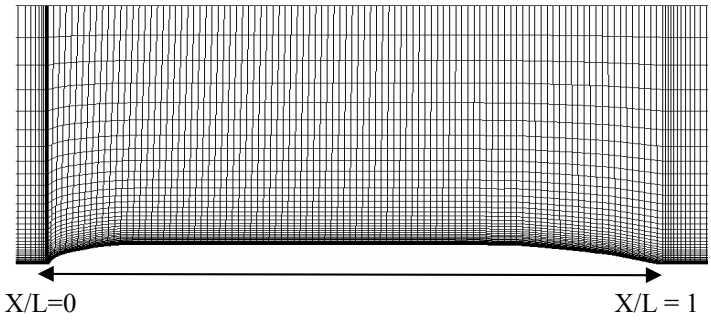

Fig. 2: Typical Grid layout of AFTERBODY1

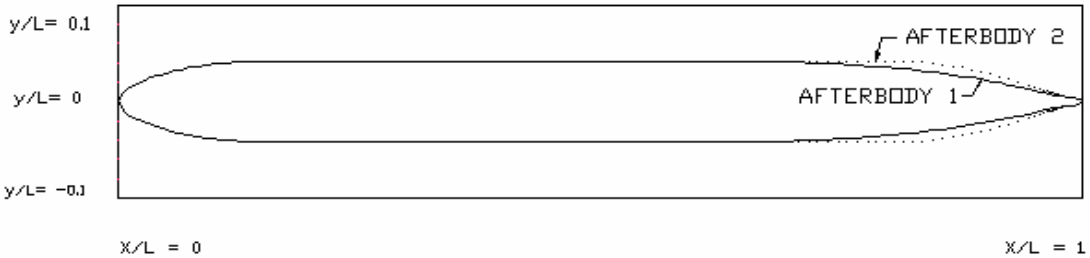

Fig. 3: Selected AUV hull forms for testing [Ref. Huang et al., (1978)]

Figure 4 displays the pressure surface boundary layer in terms of normalized velocity profiles at X/L =0.934, predicted using each mesh. The velocity profiles predicted using Grid 2 and Grid3 are identical and show clear differences from those of Grid 4 and Grid 5, again suggesting grid independence with the two finest meshes.

Therefore, with grid 2 and grid 3 predicting almost identical results, it is concluded that Grid 3 itself shows a suitable degree of grid independence. In consideration of the computing resources and time

constraints, it was concluded that the marginal performance advantage provided by the finest grid (Grid2) did not justify the increased cell numbers 100 % and extended CPU processing times. Henceforth, all numerical solutions discussed were obtained using Grid3.

Table V: Grid independence analysis-grid size and C_{dv}

Grid type	Grid size	C_{dv}	Experimental drag coefficient	% Deviation
Grid 1	342 x 96	0.0284	0.0276	2.90
Grid 2	242 x 68	0.0284		2.90
Grid 3	171 x 48	0.0290		5.07
Grid 4	121 x 34	0.0307		11.23
Grid 5	86 x 24	0.0329		16.11

Surface pressure distribution, overall volumetric drag coefficients, axial and radial velocities are important quantities for assessing the hydrodynamic efficiency of underwater hull forms. Hence any criteria developed for numerical simulation of the flow past underwater vehicle hull forms has the capability to predict these quantities with reasonable accuracy.

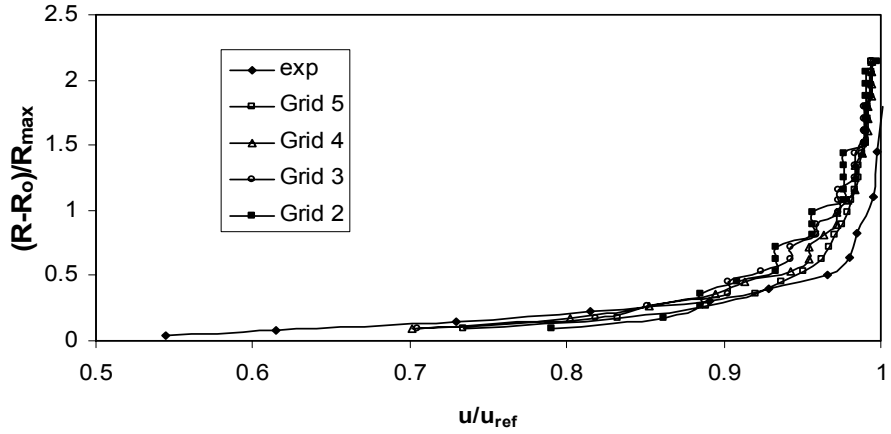

Fig. 4: Grid independence analysis: Normalized stream wise mean velocity profile at X/L = 0.934 of the pressure surface boundary layer

5.2 Performance of Turbulence models

The performance of each turbulence model is evaluated with respect to the predicted surface pressure distribution, the pressure surface boundary layer and, radial and axial velocities on the selected underwater vehicle hull forms (AUVs). All presented data are dimensionless, co-ordinate locations are referenced to the chord length (i.e. X/L), radial distance is normalized with maximum diameter of the respective body and all component velocities are normalized with the free-stream velocity.

5.2.1 Surface pressure coefficient distribution

The distribution of pressure coefficient at the surface of the underwater vehicle hull forms, as predicted by each turbulence model, at a constant free-stream velocity of 5 m/s is illustrated through Fig.5 to Fig.6. The pressure distribution predicted by all turbulence models for AFTERBODY1 and AFTERBODY2 were comparing very well with each other. Also the results are in excellent agreement with experimental results of Huang et al., (1978). The pressure distribution predicted by low-Re closure models shows a close coordination with the experimental data for all the bodies considered. However, the k-ε AKN turbulence model perform better compare to k-ε CHC, k-ε LS and k-ε YS for AFTERBODY1 (A1) and AFTERBODY2 (A2). Table VI and Table VII could better illustrate this. It could be inferred based on the figures and tables that the k-ε AKN model predicts better than all other models for AFTERBODY1 and AFTERBODY2.

5.2.2 Pressure surface boundary layer

Figures 7 to 10 illustrate the numerical and experimental pressure surface pressure boundary layer at X/L= 0.934, 1, 1.057 and 1.182, predicted by all turbulence models for AFTERBODY1. The various

turbulence models compare well with each other. Also the results compare well with available experimental data at X/L = 0.934 and X/L = 1 except at X/L = 1.057 and X/L = 1.182. This is due to flow separation and formation of wake behind the body. In all the above figures (R-Ro) represents the radial distance from the body while R_{ma} is the maximum radius of the body profile. In order to quantitatively bring out the performance of various turbulence models, the deviation between the experimental results of Huang et al., (1978) and the numerical predictions are tabulated in Table VIII and Table IX. Table VIII and Table IX details the percentage deviation of surface pressure coefficient (C_p) from experiments for the pressure boundary layer (at X = 1.0L and 1.182L) of AFTERBODY1, for all turbulence models considered in the present study. The tables suggest the maximum deviation of k-ε AKN is only 2% in comparison with the maximum deviation of 12% from other models at X/L = 1.0. However, the deviation in the wake region (X/L = 1.182) from all the tabulated values is comparable. The data present in Table VIII and Table IX clearly indicates the superiority of k-ε AKN model in predicting the pressure boundary layer. This will further enhance confidence on simulation capability of k-ε AKN model for underwater vehicle hull forms (AUVs).

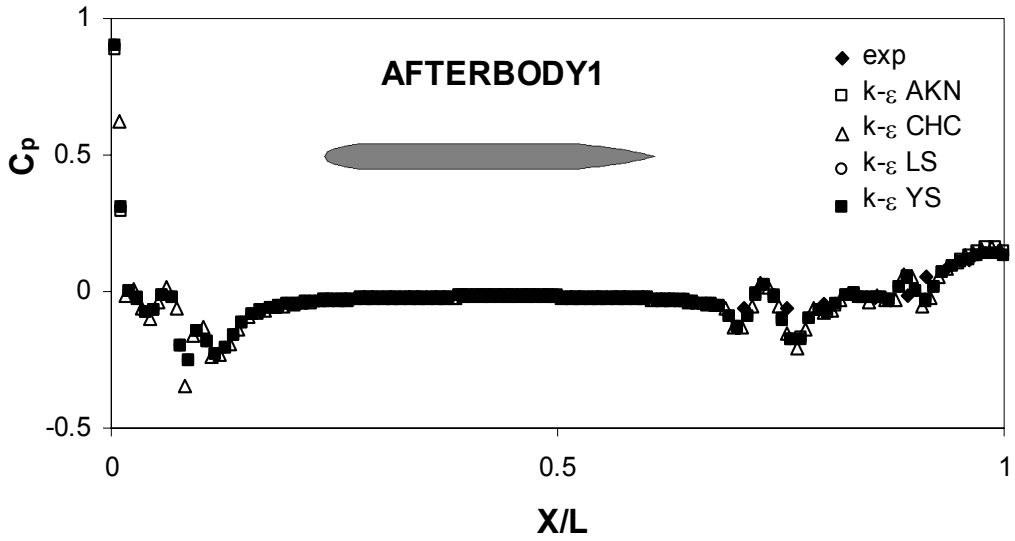

Fig. 5: Performance of various low-Re k-ε models for AFTERBODY1: Comparison of predicted pressure coefficient (C_p) with experiment values [Huang et al., (1978)]

Table VI: Volumetric drag coefficients for AFTERBODY1

Volumetric drag Coefficient	Turbulence models				Experimental drag Coefficient
	k-ε AKN	k-ε CHC	k-ε LS	k-ε YS	
C_{dv}	0.0290	0.0301	0.0319	0.0260	0.0276
C_{fv}	0.0205	0.0209	0.0225	0.0191	
C_{pv}	0.0085	0.0092	0.0094	0.0069	

Table VII: Volumetric drag coefficients for AFTERBODY2

Volumetric drag Coefficient	Turbulence models				Experimental drag Coefficient
	k-ε AKN	k-ε CHC	k-ε LS	k-ε YS	
C_{dv}	0.0297	0.0303	0.0318	0.0283	0.0280
C_{fv}	0.0189	0.0191	0.0207	0.0172	
C_{pv}	0.0108	0.0112	0.0111	0.0111	

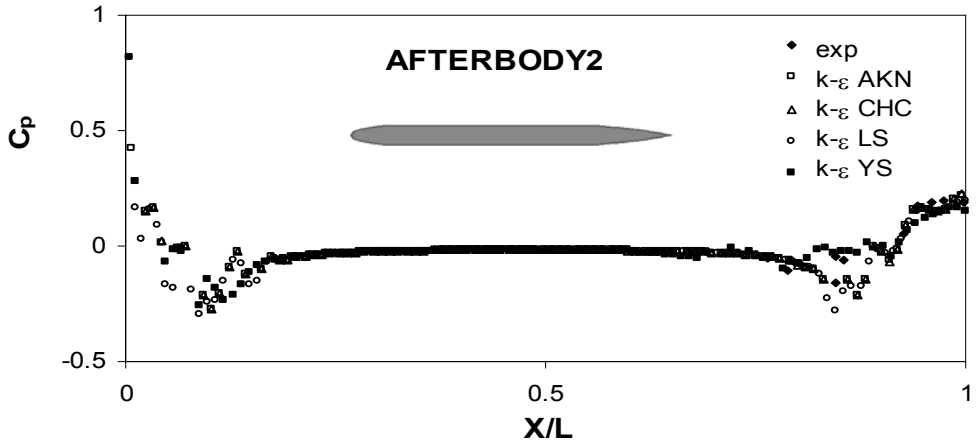

Fig. 6: Performance of various low-Re k-ε models for AFTERBODY2: Comparison of predicted pressure coefficient (C_p) with experiment values [Huang et al., (1978)]

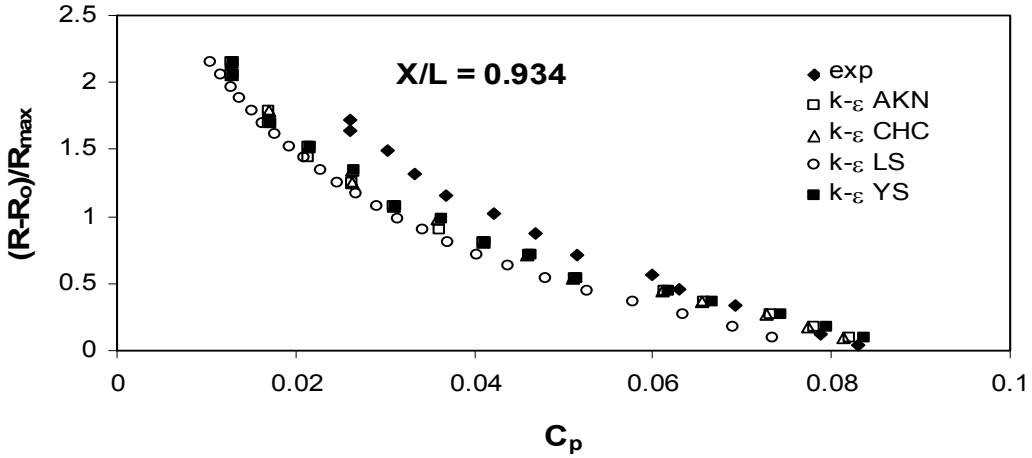

Fig. 7: Performance of various low-Re k-ε models for AFTERBODY1: Comparison of pressure coefficient (C_p) in the pressure-surface boundary layer with experiment values at X = 0.934L [Huang et al., (1978)]

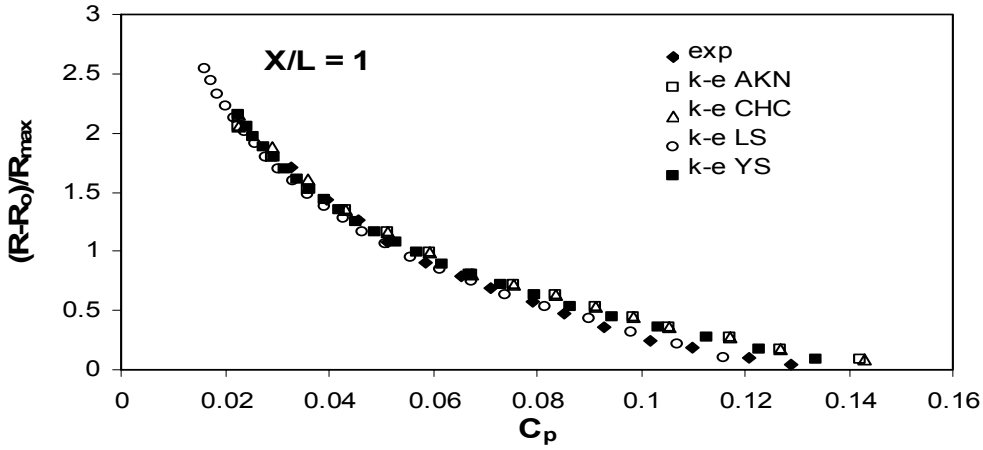

Fig. 8: Performance of various low-Re k-ε models for AFTERBODY1: Comparison of pressure coefficient (C_p) in the pressure-surface boundary layer with experiment values at X = 1.0L [Huang et al., (1978)]

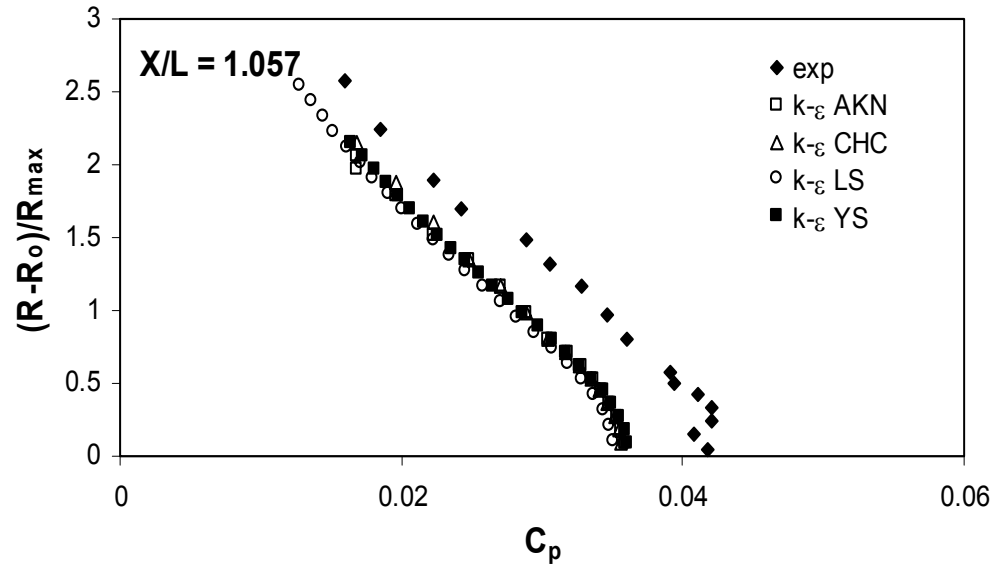

Fig. 9: Performance of various low-Re k-ε models for AFTERBODY1: Comparison of pressure coefficient (C_p) in the pressure-surface boundary layer with experiment values at X = 1.057L [Huang et al., (1978)]

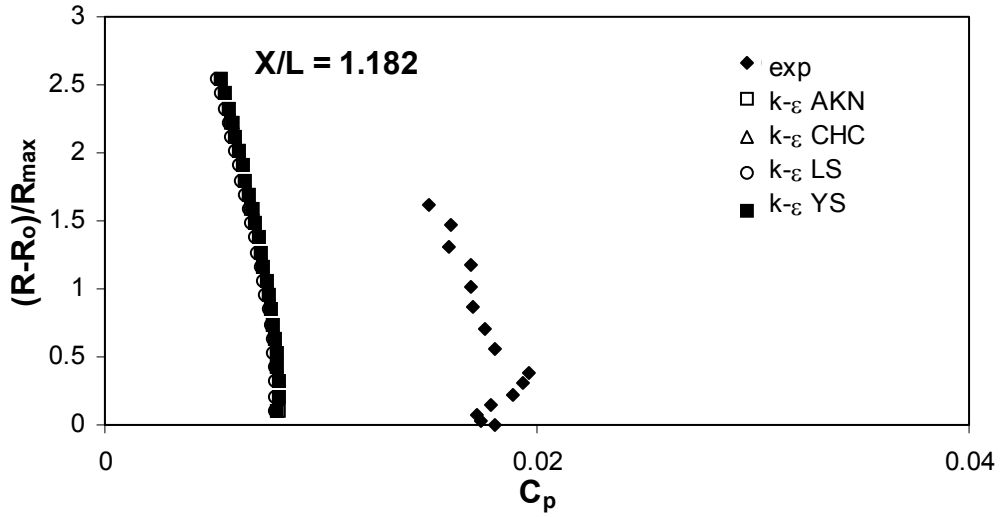

Fig. 10: Performance of various low-Re k-ε models for AFTERBODY1: Comparison of pressure coefficient (C_p) in the pressure-surface boundary layer with experiment values at X = 1.182L [Huang et al., (1978)]

5.2.3 Radial and Axial Velocity

Figures 11 to 14 illustrate the radial and axial velocity components based on numerical and experimental radial and axial component velocity boundary layer at X/L = 0.846, 0.934, 1.057 and 1.182, predicted by all turbulence models for AFTERBODY1 and the various turbulence models compare well with each other. Also the results are in excellent agreement with the experimental data. However, a meticulous examination shows that there is a definite tendency for an over prediction near the wall in the thick stern boundary layer. This is especially true for k-ε CHC, k-ε LS and k-ε YS. This is again consistent with the results of the wall pressure surface boundary layer profiles presented above and mean-velocity profiles presented below and together they suggest a need for further refinement of turbulence modeling.

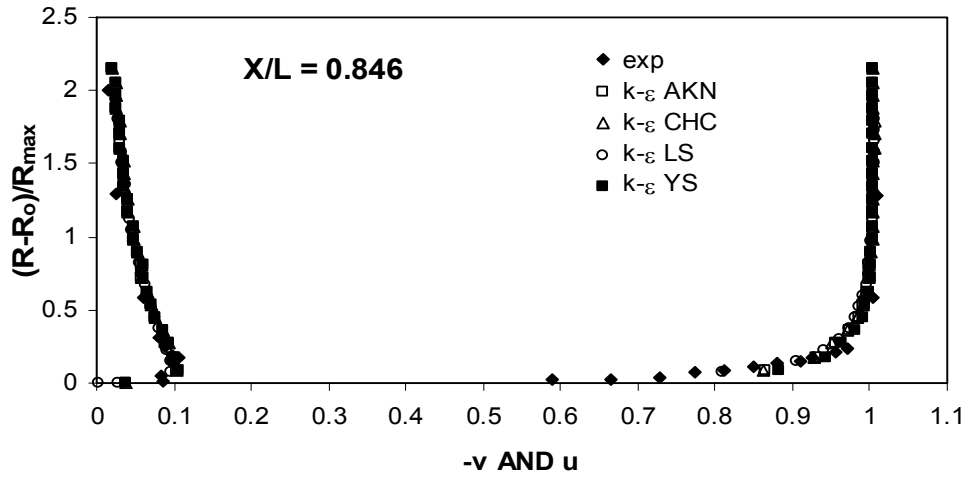

Fig. 11: Performance of various low-Re k-ε models for AFTERBODY1: Comparison of radial and axial velocities in the pressure surface boundary layer with experiment values at X = 0.846L [Huang et al., (1978)]

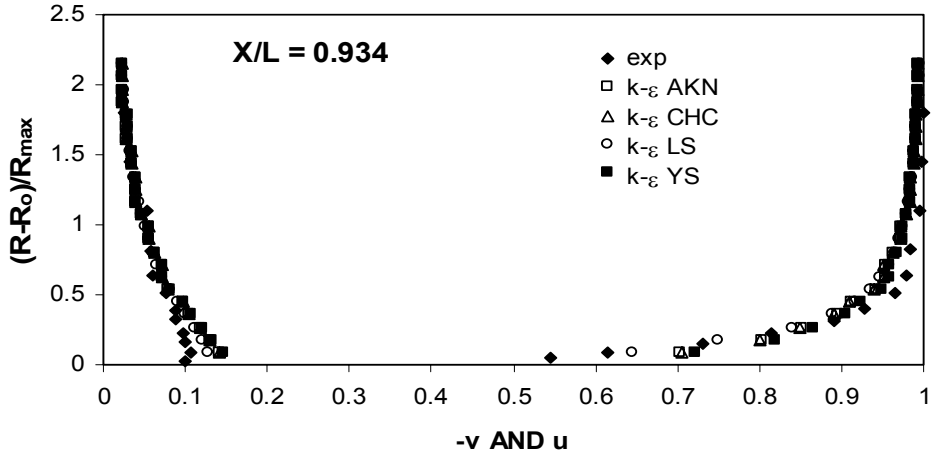

Fig. 12: Performance of various low-Re k-ε models for AFTERBODY1: Comparison of radial and axial velocities in the pressure surface boundary layer with experiment values at X = 0.934L [Huang et al., (1978)]

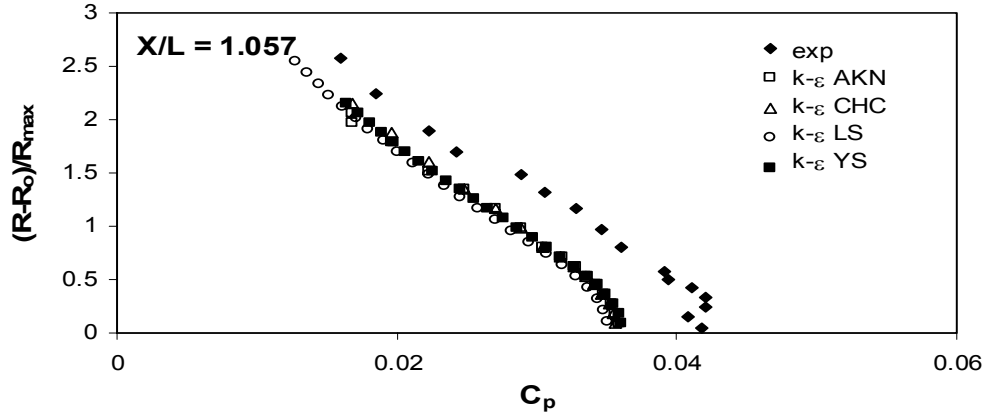

Fig. 13: Performance of various low-Re k-ε models for AFTERBODY1: Comparison of radial and axial velocities in the pressure surface boundary layer with experiment values at X = 1.057L [Huang et al., (1978)]

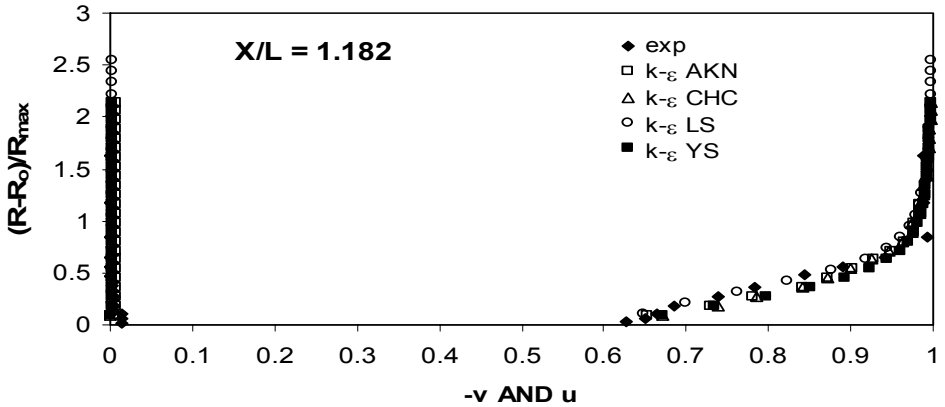

Fig. 14: Performance of various low-Re k-ε models for AFTERBODY1: Comparison of radial and axial velocities in the pressure surface boundary layer with experiment values at X = 1.182L [Huang et al., (1978)]

The foregoing discussions suggest that the k-ε AKN low-Re turbulence model may have better predicted the parameters considered. In order to clearly bring out the superior performance of k-ε AKN, the results of k-ε AKN alone are plotted with experimental results in Figs. 15 to 17 for surface pressure coefficient, pressure surface boundary layer and, radial and axial velocities respectively. These figures bring out the superior performance of k-ε AKN low-Re turbulence model by way of better comparison with experimental data as already clearly brought in Tables VIII & IX.

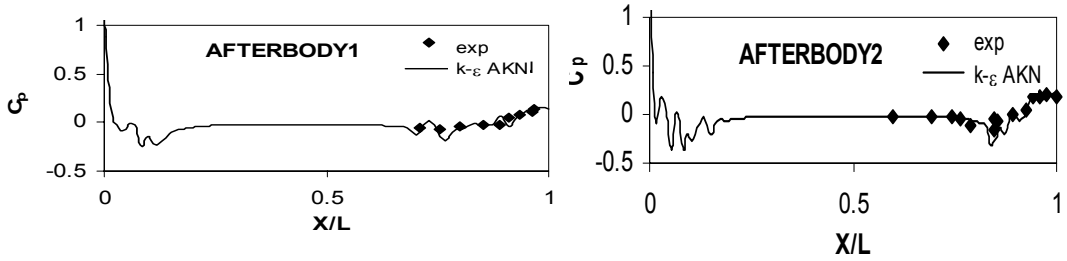

Fig. 15: Performance of k-ε AKN turbulence model for AFTERBODY1 and AFTERBODY2: Comparison of predicted pressure coefficient (C_p) with experimental values [Huang et al., (1978)]

Table VIII: Absolute percentage deviation of CFD simulated surface pressure coefficient with experiment (C_p) values for pressure boundary layer at X/L = 1.0 (AFTERBODY1)

$(R-R_o)/R_{max}$	Percentage deviation of simulated with experiment (C_p) values			
	k-ε AKN	k-ε CHC	k-ε LS	k-ε YS
0.1835	0.09	15.00	0.09	11.44
0.2414	0.02	23.47	3.00	13.71
0.3597	1.00	13.00	7.00	11.00
0.4741	0.13	1.31	0.60	0.84
0.5760	2.00	11.60	2.24	5.40
0.6924	0.85	12.22	8.01	4.73
0.7943	0.24	4.77	1.66	3.91
0.9107	0.68	7.22	2.71	4.50
1.0710	1.09	7.50	6.83	3.00
1.2606	3.13	10.01	5.22	10.01
1.4356	0.57	2.70	5.80	1.01
1.7129	2.05	1.61	8.32	5.12

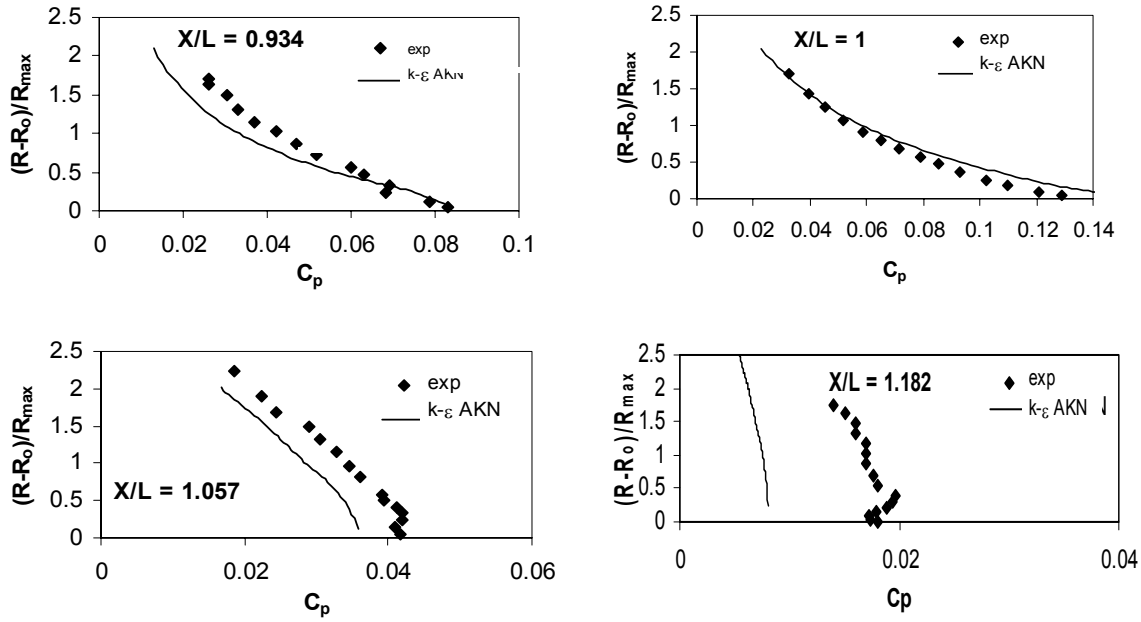

Fig. 16: Performance of k-ε AKN turbulence model for AFTERBODY1: Comparison of pressure coefficient (C_p) in the pressure-surface boundary layer with experiment values at X/L = 0.934, 1, 1.057 & 1.182 [Huang et al., (1978)]

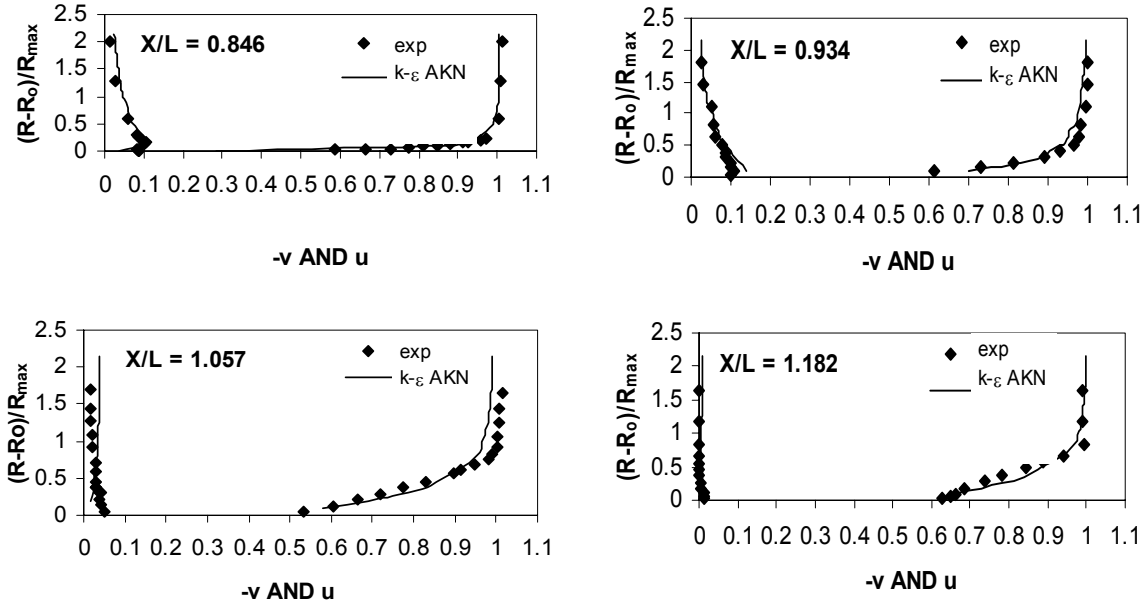

Fig. 17: Performance of k-ε AKN turbulence model for AFTERBODY1: Comparison of radial and axial velocities in the pressure surface boundary layer with experiment values at X/L = 0.846, 0.934, 1.057 & 1.182 [Huang et al., (1978)]

5.3 Superiority of k-ε AKN turbulence model

The suitability of four low-Re k-ε models for simulation of flow past two typical underwater vehicle hull forms is investigated under this study. These investigations are restricted to computation of the total volumetric drag coefficient, surface pressure coefficient distribution and, pressure and velocity boundary layers. Reasonable resolution of the turbulent boundary around the vehicle surface is

guaranteed by placing the first node at y^+ =2 and five nodes with in y^+ =11.5. Along with the above criterion 101 nodes along the body profile having a growth ratio of 1:1 and 48 nodes in the radial direction having a growth rate of 1:1.17 beyond laminar sub layer (y^+ =11.5) will ensure grid convergence. The above observations are limited to low-Re turbulence models considered in this study. Analysis of the turbulent boundary on the pressure surface of the underwater vehicle surfaces show that the k-ε AKN model accurately resolves the surface pressure coefficient profiles, pressure boundary layers and velocity profiles for underwater vehicle hull forms (AUVs). It also predicts well the boundary layer separation from the trailing edge (Figs. 15-17 and Tables VIII- IX).

Table IX: Absolute percentage deviation of CFD simulated surface pressure coefficient with experiment (C_p) values for pressure boundary layer at X/L = 1.182 (AFTERBODY1)

$(R-R_o)/R_{max}$	Percentage deviation of simulated with experiment (C_p) values			
	k-ε AKN	k-ε CHC	k-ε LS	k-ε YS
0.1491	55.00	55.17	56.00	55.23
0.2214	57.52	57.58	58.36	58.00
0.3090	54.58	58.63	59.39	58.65
0.3886	59.21	59.23	59.94	59.25
0.5540	56.10	56.15	56.81	56.14
0.7045	55.66	55.68	56.35	56.00
0.8627	54.93	55.00	55.70	55.00
1.0135	55.79	56.00	56.61	56.00
1.1722	56.76	57.00	58.00	58.00
1.3143	55.00	55.43	56.11	55.17
1.4651	56.51	57.10	57.51	57.00
1.6230	55.00	55.05	56.13	55.10
1.7492	53.00	53.23	54.29	53.16

As for the turbulence modeling, the k-ε AKN low-Re turbulence model works even in the vicinity of the wall and more precisely reproduces the near-wall limiting behavior (laminar sublayer growth) and provides accurately the effect of pressure gradient for the turbulent flows considered. In k-ε AKN model while defining the non-dimensional distance y^k, $u_\varepsilon = \gamma\varepsilon^{1/4}$ is used instead of friction velocity u_τ to account for the near-wall and low-Reynolds-number effects. The velocity scale u_ε becomes zero neither at the separating nor at the reattaching points in contrast to the frictional velocity u_τ. In addition to these, major modifications done in the model functions f_μ, f_1 and f_2, and reevaluated model constants being used, i.e. $c_\mu = 0.09$, $\sigma_k = 1.4$, $\sigma_\varepsilon = 1.4$, $c_{\varepsilon 1} = 1.5$ and $c_{\varepsilon 2} = 1.9$ (Abe et al., 1994) in the transport equation for the turbulent energy and its dissipation rate are the reasons for improvement of accuracy.
As a resultant of these modifications, k-ε AKN predicts, quite successfully, the mean, separated and reattaching flows, which in turns leads to good prediction of overall volumetric drag coefficients, surface pressure coefficients, and axial and radial velocities of underwater axisymmetric bodies, when applied in the steady state condition.

6. Conclusions

A comparative evaluation of the four low-Re k- ε models (i.e. k-ε AKN, k-ε CHC, k-ε LS and k-ε YS) using standard CFD solver FLUENT® 6.1.

1. The investigation revealed that the k-ε AKN turbulent model shows vastly superior performance when applied in the steady-state analysis of underwater vehicle hull form (AUVs) at Re between 6.6 x 10^6 and 6.80 x 10^6 and at a speed of 5 m/s.
2. The requirements of boundary layer resolution for low-Re turbulent models are that the first grid should be at y^+ = 2 and at least 5 nodes must lie with in the laminar boundary layer. Grid convergence is achieved by resolving the body lengths by more than 100 nodes.
3. The k-ε AKN turbulence model has also well predicted the total volumetric drag coefficients, surface pressure coefficients, pressure and velocity boundary layers for the two bodies considered.
4. The analysis also revealed that the k-ε AKN model predicts the flow separation and wake formation more closely than the other models considered.

Acknowledgments

The authors express their gratitude towards Indian Institute of Technology Madras for providing necessary facilities.

References

Abe, K., Kondoh, T. and Nagano, Y. (1994): A new turbulence model for predicting fluid flow and heat transfer in separating and reattaching flows – 1. Flow field calculations, Int .J. Heat and Mass Transfer. Vol.37, No.1, pp. 139 -151.

Chang, K.C., Hsieh, W.D. & Chen, C.S. (1995): A modified low-Reynolds-number turbulence model applicable to recirculating flow in pipe expansion, Journal of Fluid Engineering, Vol. 117, pp. 417-423.

Choi, S.K, Chen and C.J. (1990): Laminar and turbulent flows past two dimensional and axisymmetric bodies, Iowa Institute of Hydraulic Research, IIHR Report 334-II.

Choi, S.K. and Chin, J.C. (1991): Navier-Stokes Solution of Complete Turbulent Flow past Finite Axisymmetric Bodies, AIAA Journal, Vol.29, No.6, pp. 998-1001.

Lam, C.K.G. and Bremhorst, K. (1981): A modified form of the k-e model for predicting wall turbulence, ASME Journal Fluid Engineering, Vo.103, p. 456.

Launder, B. and Sharma, B. (1974): Application of the energy dissipation model of turbulence to the calculation of flow near a spinning disc, Lett. Heat and Mass transfer, Vol. 1, pp. 131-138.

Launder, B.E. and Spalding, D.B. (1974): The Numerical Calculation of Turbulent Flows, Computer Methods in Applied Mechanics and Engineering, 3 (2), 269-289.

Huang, T.T., Santelli, N. and Belt, G. (1978): Stern Boundary-Layer Flow on Axisymmetric Bodies, In proceedings of the 12th ONR Symposium on Naval Hydrodynamics, Washington, D.C., pp. 127-157.

Oh, C.S. & Choi, D.H. (1997): An improved Navier-Stokes procedure for analysis of two-dimensional aerofoil in laminar and turbulent flows. International Journal of Numerical Methods in fluids, Vol. 25, pp. 167-182.

Patel, V.C. (1973): A simple integral method for the calculation of thick axisymmetric boundary layers, Iowa Institute of Hydraulic Research, IIHR Reprot 150.

Patel, V.C. (1973): On the Equation of a Thick Axisymmetric Turbulent Boundary Layer, Iowa Institute of Hydraulic Research. IIHR Report 143.

Patel, V.C., Rodi, W. and Scheurer, G. (1984): Turbulence models for near-wall and low-Reynolds number flows: A review, AIAA Journal. Vol. 23, No. 9, pp. 1308-1318.

Patel, V.C. and Chen, H.C. (1986): Flow Over Tail and in Wake of Axisymmetric Bodies: Review of the State of the Art, Journal of Ship Research, Vol. 30, No. 3, pp. 202-314.

Sarkar, T., Sayer, P.G. and Fraser S.M. (1997): Flow simulation past axisymmetric bodies using four different turbulence models, Journal of Applied Mathematical Modeling. Vol. 21, pp. 783-792.

Sarkar, T., Sayer, P.G. and Fraser S.M. (1997): A study of autonomous underwater vehicle hull forms using computational fluid dynamics, International Journal for Numerical Methods in Fluids, Vol. 25, pp. 1301-1313.

Schlichting, H & Gersten, K. (2000): Reprint Boundary Layer Theory (8th edn), Springer, India.

Stern, F., Wilson, R.V. & Coleman, H.W. & Paterson, E.G. (1999): Verification and validation of CFD simulations, Iowa Institute of Hydraulic Research, IIHR Report 407.

Yang, Z., and Shih, T.H. (1993): New time scale based k-ε model for near-wall turbulence, AIAA Journal, Vol. 31, No.7, pp. 1191 – 1198.